Real-World Image Super-Resolution as Multi-Task Learning

Wenlong Zhang^{1,2}, Xiaohui Li^{2,3}, Guangyuan Shi^{1}, Xiangyu Chen^{2,4,5}
Xiaoyun Zhang^{3}, Yu Qiao^{2,5}, Xiao-Ming Wu^{1}†, Chao Dong^{2,5}†
^{1}The HongKong Polytechnic University ^{2}Shanghai AI Laboratory
^{3}Shanghai Jiao Tong University ^{4}University of Macau
^{5}Shenzhen Institute of Advanced Technology, CAS
`wenlong.zhang@connect.polyu.hk, xiao-ming.wu@polyu.edu.hk, chao.dong@siat.ac.cn`

Abstract

In this paper, we take a new look at real-world image super-resolution (real-SR) from a multi-task learning perspective. We demonstrate that the conventional formulation of real-SR can be viewed as solving multiple distinct degradation tasks using a single shared model. This poses a challenge known as task competition or task conflict in multi-task learning, where certain tasks dominate the learning process, resulting in poor performance on other tasks. This problem is exacerbated in the case of real-SR, due to the involvement of numerous degradation tasks. To address the issue of task competition in real-SR, we propose a task grouping approach. Our approach efficiently identifies the degradation tasks where a real-SR model falls short and groups these unsatisfactory tasks into multiple task groups. We then utilize the task groups to fine-tune the real-SR model in a simple way, which effectively mitigates task competition and facilitates knowledge transfer. Extensive experiments demonstrate our method achieves significantly enhanced performance across a wide range of degradation scenarios. The source code is available at `https://github.com/XPixelGroup/TGSR`.

1 Introduction

Real-world image super-resolution (real-SR) aims to enhance the resolution and quality of low-resolution images captured in real-world scenarios. Real-SR algorithms enable improved image quality and better visual understanding, making them valuable in a wide range of applications [43, 46, 45, 14, 17]. Unlike non-blind SR [9, 56, 55] and classical blind SR [13, 18, 38] that assumes a simple degradation process, real-SR deals with complex and unknown degradations present in real-world imaging conditions, such as noise, blur, compression artifacts, and sensor limitations. The diversity of real-world degradations and unknown degradation parameters make it challenging to reverse the specific degradation effects and accurately recover high-resolution details.

Prior studies tackle real-SR by designing various degradation models to simulate the degradation process in real-world scenarios. For instance, they generate synthetic paired training data with a shuffled degradation model (BSRGAN [50]), a high-order degradation model (RealESRGAN [39]), or a three-level degradation model (DASR [25]). Existing methods commonly train a single real-SR network with training data generated by a sophisticated degradation model, aiming to cover as many degradation cases as possible during the training process. Under this framework, recent works have focused on enhancing various aspects of the real-SR network, including improving the backbone network architecture [26], optimizing inference efficiency [25], enhancing generalization capabilities [23], and improving modulation ability [31].

†Corresponding author

This study takes a new look at real-SR from a multi-task learning perspective. We show that the conventional formulation of real-SR essentially corresponds to a multi-task learning problem, which involves solving a large number of different degradation tasks simultaneously with a single shared model. Consequently, real-SR faces a well-known challenge in multi-task learning, namely *task competition or task conflict* [32]. It refers to the situation that tasks compete for model capacity, potentially resulting in certain tasks dominating the learning process and adversely affecting the performance of other tasks. This problem is severely aggravated in the case of real-SR, where a large number of degradation tasks (up to thousands) are typically involved. In our pilot experiment (Fig. 1), we have observed that a real-SR network trained with the multi-task objective fails to yield satisfactory results for a significant portion of degradation tasks.

We propose a task grouping approach (Fig. 2) to alleviate the negative impact of task competition for real-SR. Task grouping [48, 37, 35, 10] is an effective technique in multi-task learning that helps mitigate negative transfer by training similar tasks together. This approach typically involves learning the relationship or relevance between pairs of tasks through validation or fine-tuning, which becomes impractical in the context of real-SR where there is a large number of tasks to consider. Hence, we resort to design indirect measures to assess task affinity. Specifically, we introduce a performance indicator based on gradient updates to efficiently identify the degradation tasks that a real-SR model falls short of. Then, we propose an algorithm to group these unsatisfactory tasks into multiple groups based on a performance improvement score. Finally, we propose TGSR, a simple yet effective real-SR method, which leverages the identified task groups to fine-tune the pre-trained real-SR network. Our key contributions are summarized as follows:

- We take a new look at real-SR from a multi-task learning perspective and highlight the task competition problem.
- We propose a task grouping approach to effectively address the task competition problem for real-SR and develop a task grouping based real-SR method (TGSR).
- We conduct extensive experiments to validate the effectiveness of TGSR, and the results demonstrate its superior performance compared to state-of-the-art real-SR methods.

2 Related Work

Image super-resolution. Since Dong *et al.* [9] first introduced Convolutional Neural Networks (CNNs) to the SR problem, a series of learning-based SR methods have made great progress, including deep networks [21], dense connections [56], channel attention of [55], residual-in-residual dense blocks [41], and transformer structure [26]. To reconstruct realistic textures, Generative Adversarial Networks (GANs) [24, 41, 53, 42] have been employed to generate visually pleasing results. However, these methods adopt a bicubic down-sampling degradation that is insufficient for real-world images.

Real-world super-resolution. To address the SR problem in real-world scenarios, classical blind SR methods primarily use Gaussian blur and noise to model the distribution of real-world images. Significant progress has been made through a variety of approaches, including the use of a single SR network with multiple degradations [51], kernel estimation [13, 18, 44, 2], and representation learning [38]. Additionally, BSRGAN [50] proposes a large degradation model that incorporates multiple degradations using a shuffled strategy, while RealESRGAN [39] employs a high-order strategy to construct a large degradation model. DASR [25] adopts a three-level degradation distribution (i.e., two one-order and one high-order degradation models) to simulate the distribution of real-world images. These works demonstrate the potential of large degradation models for real-world applications. In addition, recent works also improve real-SR in multiple dimensions, such as network backbone [26], efficiency [25], generalization [23, 54, 52] and modulation ability [31].

Multi-task learning. Multi-task learning methods can be roughly divided into three categories: task balancing, task grouping, and architecture design. Task balancing [16, 20, 47, 27, 34, 15, 8, 7, 19] methods address task/gradient conflicts by re-weighting the loss or manipulating the update gradient. Task grouping [48, 37, 35, 10] methods mainly focus on identifying which tasks should be learned together. Zamir et al. [48] provide a task taxonomy that captures the notion of task transferability. TAG [10] determines task groups by computing affinity scores that capture the effect between tasks. Architecture design methods can mainly be divided into hard parameter sharing methods [22, 28, 3] and soft parameter sharing methods [30, 33, 12, 11]. Hard parameter sharing methods require

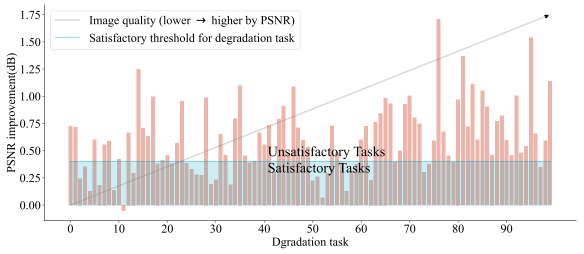

(a) PSNR distance between the real-SR and single-task SR networks across 100 randomly selected degradation tasks.

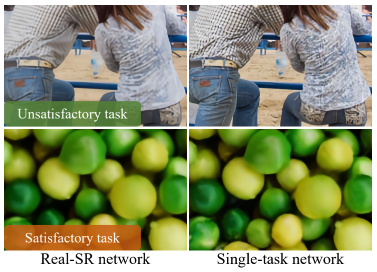

(b) Visual comparison between satisfactory and unsatisfactory tasks.

Figure 1: **Illustration of task competition.** The jointly-trained multi-task real-SR network falls short in producing satisfactory results for almost half of the degradation tasks, on which the fine-tuned single-task networks obtain more than 0.4dB performance gain, indicating these tasks are dominated by other tasks during the learning process.

different decoders for different tasks, while soft parameter sharing methods do cross-talk between different task networks. We focus on a task grouping strategy in our TGSR. The strategy identifies unsatisfactory degradation tasks in a large degradation space. Subsequently, we can further improve the overall performance of the real-SR network by fine-tuning it in the unsatisfactory tasks.

3 Real-SR as a Multi-task Learning Problem

Problem Formulation Real-SR aims to restore a high-resolution (HR) image x from its low-resolution (LR) counterpart y that has undergone an unknown and intricate degradation process:

$$y = \mathcal{D}(x) = (f_n \circ \cdots \circ f_2 \circ f_1)(x), \tag{1}$$

where f_i represents a degradation function such as Gaussian blurring with a kernel width [0.1, 2.4], adding Gaussian noise with a noise level [1, 25], a downsampling operation with a scale factor r, or applying the JPEG compression. Hence, $\mathcal{D}$ represents a vast continuous degradation space that encompasses an infinite number of degradations. Existing real-SR models such as BSRGAN [50], RealESRGAN [39], and DASR [25] make different assumptions in the generation of $\mathcal{D}$, aiming to simulate the highly complex degradation process in real-world scenarios.

An SR task τ can be defined as a training pair $(x, y = d(x))$ formed by sampling a degradation d from the degradation space $\mathcal{D}$ and applying it on an HR image x to generate an LR image y. Due to the infinite size of $\mathcal{D}$, it is impossible to consider every degradation case. Hence, a common approach is to sample a large number of degradations to sufficiently represent the degradation space. Given a set of high-resolution images $\mathcal{X}$, with N different degradations sampled from $\mathcal{D}$ ($N \gg |\mathcal{X}|$), we can generate a set of SR tasks: $\mathcal{T} = \{\tau_i = (x_i, y_i)\}_{i=1}^N$, where $x_i \in \mathcal{X}$ and y_i is obtained by applying a degradation on x_i. A real-SR model is commonly trained by minimizing the empirical risk:

$$\mathcal{L}_{\text{total}}(\theta) = \sum_{i=1}^{N} \mathcal{L}_i(\tau_i; \theta), \tag{2}$$

where $\mathcal{L}_i$ is the loss on task τ_i, and θ are the trainable model parameters shared by all N tasks. Therefore, real-SR is essentially a multi-task learning problem, aiming to solve N different SR tasks with a single shared model. In the following, we refer to τ_i as a *degradation task*.

Task Competition From the view of multi-task learning, real-SR is a challenging problem as it intends to solve a large number of different degradation tasks (e.g., $N = 10^3$) altogether with a single model, inevitably suffering from task competition that some tasks may dominate the training process leading to poor performance on other tasks [37].

To illustrate the impact of task competition, we randomly sample 100 degradation tasks with the degradation model in [39] and train a real-SR network with the multi-task objective in Eq. 2. Next, we fine-tune the real-SR network on each degradation task independently and obtain 100 fine-tuned

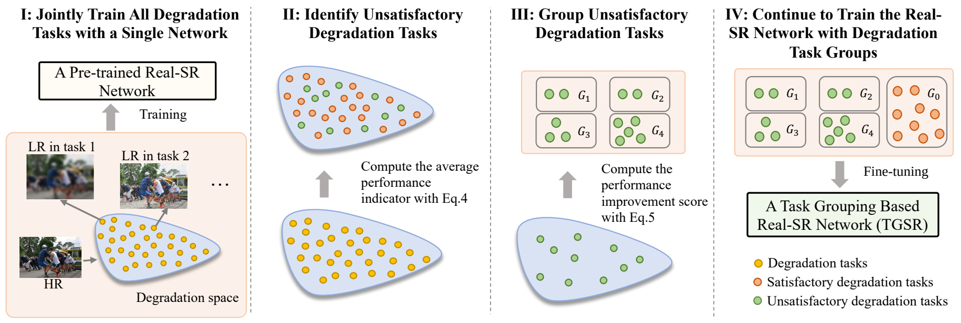
I: Jointly Train All Degradation Tasks with a Single Network
A Pre-trained Real-SR Network
Training
LR in task 1
LR in task 2
HR
Degradation space
II: Identify Unsatisfactory Degradation Tasks
Compute the average performance indicator with Eq.4
III: Group Unsatisfactory Degradation Tasks
Compute the performance improvement score with Eq.5
IV: Continue to Train the Real-SR Network with Degradation Task Groups
Fine-tuning
A Task Grouping Based Real-SR Network (TGSR)
Degradation tasks
Satisfactory degradation tasks
Unsatisfactory degradation tasks

Figure 2: Overview of our proposed task grouping approach for real-SR.

models, which we call single-task networks. We then compare the performance between the real-SR network and the single-task networks on each degradation task by computing their PSNR distance. The results in Fig. 1 show that for nearly half of the degradation tasks, the PSNR distance between the real-SR network and single-task network exceeds 0.4dB, indicating that these tasks are not well solved by the real-SR network, which we refer to as *unsatisfactory tasks*. From an optimization perspective, the other tasks (those with PSNR distance less than 0.4dB) dominate the learning process and are effectively solved by the real-SR network, which we refer to as *satisfactory tasks*.

4 Real-SR via Task Grouping

Our analysis in Sec. 3 shows that when a real-SR network is tasked with many degradation tasks, they may compete for model capacity or interfere with each other, resulting in a significant decline in performance for certain tasks. This phenomenon, commonly referred to as *negative transfer* [37], is a well-known challenge in the field of multi-task learning. An effective approach to mitigate negative transfer is task selection or task grouping [10, 37, 48]. By finding groups of tasks that may benefit from training together, the interference among tasks can be minimized.

4.1 Which Tasks Should Be Learned Together for Real-SR?

The results in Fig. 1 suggest that the satisfactory tasks should be grouped together. These dominant tasks may share certain characteristics or similarities that lead to minimal task conflicts, making them more prominent in the training process. More importantly, considering that the real-SR network has effectively tackled these tasks and reached a satisfactory performance level, we may focus on the unsatisfactory tasks that present greater potential for improvement.

Efficiently Identifying Unsatisfactory Tasks To identify the unsatisfactory tasks, we may use the approach described in Sec. 3 and Fig. 1, by comparing the performance between the jointly-trained multi-task real-SR network (referred to as the *pre-trained* real-SR network hereafter) and the fine-tuned single-task networks. However, the cost of adopting this approach is prohibitive due to the large number of degradation tasks (e.g., thousands or tens of thousands) involved in real-SR.

Therefore, to efficiently identify the unsatisfactory tasks, we propose a measure to assess whether a degradation task has been well solved by the real-SR network, which is done through fine-tuning the pre-trained real-SR network for a small number of iterations (e.g., 100) on the degradation task. Specifically, we assess the impact of the gradient update of task τ_i on the shared parameters θ (i.e., the pre-trained real-SR network), by comparing the loss of τ_i before and after updating θ. We develop a *performance indicator* defined as:

$$z_i^t = \frac{\mathcal{L}_i(\tau_i, \theta_i^t)}{\mathcal{L}_i(\tau_i, \theta)}, \tag{3}$$

where θ_i^t are the parameters updated on task τ_i at the time step t. Notice that a high value of z_i^t indicates the loss of task τ_i is not significantly reduced after fine-tuning, suggesting that the pre-trained real-SR network has achieved good performance on this task.

Algorithm 1: Degradation Task Grouping for Real-SR

```
Input: A set of degradation tasks $\mathcal{T} = \{\tau_1, \tau_2, ..., \tau_n\}$, the pre-trained real-SR model $\theta$, the
       number of groups $c$, and the threshold values $t_0, t_1, \cdots, t_c$.
for any $\tau_i \in \mathcal{T}$ do
    Compute the average performance indicator $\hat{z}_i$ with Eq. 4;
end
// Select unsatisfactory tasks
Let $\hat{\mathcal{T}} = \{\tau_i | \hat{z}_i > t_0\}$ ;
// Group unsatisfactory tasks
for $i = 1, \ldots, c$ do
    Fine-tune the pre-trained real-SR network with all unsatisfactory tasks;
    for any $\tau_j \in \hat{\mathcal{T}}$ do
        Compute the performance improvement score $s_j$ with Eq. 5;
    end
    Let $G_i = \{\tau_j | s_j > t_i\}$, where $t_i$ is the threshold for group $i$;
    Let $\hat{\mathcal{T}} = \hat{\mathcal{T}} \backslash G_i$;
end
Output: Degradation task groups $\mathcal{G} = \{G_1, G_2, .., G_c\}$.
```

For stability, we consider the average performance indicator during the fine-tuning process on task τ_i:

$$\hat{z}_i = \frac{1}{t_e - t_s} \sum_{t=t_s}^{t_e} z_i^t, \tag{4}$$

where t_s and t_e represent the starting and end points of a time span, respectively. With the computed average performance indicator of each task, we can set a threshold to select the unsatisfactory tasks. The effectiveness of $\hat{z}_i$ is validated in Sec. 5.2 and Sec. 5.3.

Grouping Unsatisfactory Tasks into Multiple Task Groups The number of identified unsatisfactory degradation tasks can still be significant, typically in the range of hundreds in our experiments. Given the potential variance among these tasks, it would be advantageous to further divide them into multiple task groups based on their similarity to reduce negative transfer. A common approach for task grouping in multi-task learning is to learn pairwise performance indicator between tasks [48, 10, 37], which is impractical for real-SR due to the large number of degradation tasks involved.

A feasible way is to learn an indirect measure of task similarity by fine-tuning the pre-trained real-SR network on each degradation task independently and computing the PSNR distance as described in Sec. 3 and Fig. 1. However, this approach is still time-consuming given the large number of unsatisfactory tasks. Another alternative of indirect measure is the average performance indicator in Eq. 4, which, although efficient, may not be accurate enough. Hence, we make a trade-off to fine-tune the pre-trained real-SR network θ on all unsatisfactory tasks simultaneously through joint-training to obtain a new network $\hat{\theta}$. Then, we test the fine-tuned network $\hat{\theta}$ on each degradation task with an available validation set and compute a *performance improvement score (PIS)* defined as:

$$s_j = I(\mathcal{D}_j^{\text{val}}; \hat{\theta}) - I(\mathcal{D}_j^{\text{val}}; \theta), \tag{5}$$

where $\mathcal{D}_i^{\text{val}}$ represents the validation set of an unsatisfactory task τ_i, I is an IQA (image quality assessment) metric such as PSNR, and s_i is the PIS of task τ_i. We then select the tasks with PIS larger than some threshold to form a task group, which should have small conflicts as they dominate the fine-tuning process. We repeat this process to find the rest of task groups as described in Alg. 1.

4.2 TGSR: A Task Grouping Based Real-SR Method

With the identified degradation task groups $\mathcal{G} = \{G_1, G_2, .., G_c\}$, we adopt a straightforward method to fine-tune the pre-trained real-SR network, referred to as TGSR. We first form $\hat{\mathcal{G}} = \{G_0, \mathcal{G}\} = \{G_0, G_1, G_2, .., G_c\}$, where G_0 represents the entire degradation space and serves for preventing

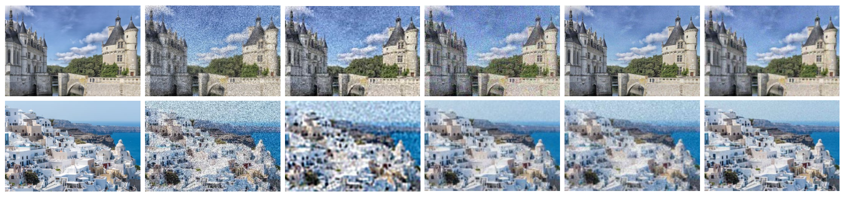

Figure 3: Sample images from different degradation task groups in our DIV2K5G datasets.

catastrophic forgetting during the fine-tuning process. Then, we randomly select a group from $\hat{\mathcal{G}}$ and randomly sample a task from the chosen group for fine-tuning. This approach effectively increases the inclusion of the unsatisfactory tasks during the fine-tuning process and weights their likelihood of being chosen based on their respective group size (i.e., tasks in smaller groups have a higher probability to be selected). In essence, it is similar to the task re-weighting approach commonly used in multi-task learning.

5 Experiments

5.1 Experimental Setup

Datasets and evaluation. We employ DIV2K [1], Flickr2K [1] and OutdoorSceneTraining [40] datasets to implement our task grouping algorithm and train the TGSR network. For evaluation, we use DIV2K validation set to construct a DIV2K5G dataset consisting of 5 validation sets according to the divided 5 different degradation groups by the task grouping algorithm, as shown in Fig. 3. Each validation set contains 100 image pairs. In addition to the task group based test set, we employ the synthetic test set AIM2019 [29] and DIV2K_random for evaluation. The DIV2K_random is generated using the RealESRGAN degradation model on the DIV2K validation set. Furthermore, we incorporate the real-world test set, RealSR set [4], into our evaluation process. All evaluations are conducted on $\times 4$ SR and PSNR is computed on the Y channel of YCbCr color space.

Implementation details. We adopt the high-order degradation model proposed by RealESRGAN [39] as the real-SR degradation model in our experiments. To compute the performance indicator, N (4×10^3) degradation tasks are sampled from the whole degradation space. The single-task network is fine-tuned from the pre-trained RealESRNet model for 100 iterations. The performance indicator is computed based on the average of the last 10 iterations considering the instability of the training procedure. To implement the degradation grouping, the degradation tasks with the top 40% higher performance indicators (1.6×10^3 degradation tasks) are selected as unsatisfactory tasks. Then, we fine-tune the pre-trained RealESRNet for 1×10^4 iterations based on all unsatisfactory tasks. After that, we evaluate the model on Set14 [49] for each unsatisfactory degradation task. By using the proposed performance improvement score, we divide the degradation tasks into five groups based on the thresholds of [0.8, 0.6, 0.4, 0.2]. According to this set of thresholds, we obtain four groups with the number of tasks in each group being [14, 29, 84, 200] as groups1-4. Then, we label the entire degradation space beyond the four degradation groups as Group0. To avoid forgetting the satisfactory tasks, we uniformly sample degradation tasks from each group to fine-tune the pre-trained real-SR network. Other basic training settings follow RealESRGAN.

5.2 Comparison with State-of-the-Art

We compare our TGSR with the state-of-the-art methods, including SRGAN [24], ESRGAN [41], RDSR [23], MM-RealSR [31] BSRGAN [50], SwinIR [26], RealESRGAN [39], DASR [25] and HAT [6, 5]. Officially released pre-trained models are used for the compared methods.

Our TGSR improves the overall performance. The quantitative results of different methods are presented in Tab. 1. ESRGAN is based on a single-degradation model (i.e., Bicubic setting), so it performs worst under the multi-degradation evaluation system. RDSR is an MSE-based method, so it achieves the highest PSNR but performs rather poorly (the second worst) performance on LPIPS. BSRGAN, RealSwinIR, and DASR employ a one-order degradation model. They sacrifice performance on PSNR for better perceptual quality (reflected in low LPIPS). MM-RealSR and

Table 1: Quantitative results of different methods on DIV2K5G. Group0 denotes the validation set with satisfactory degradation tasks, and Group1-4 represent the validation sets with unsatisfactory degradation tasks. The ESRGAN trained on the non-blind setting and RDSR trained on the MSE-based setting are marked in gray.

	Group0		Group1		Group2		Group3		Group4	
	PSNR	LPIPS	PSNR	LPIPS	PSNR	LPIPS	PSNR	LPIPS	PSNR	LPIPS
ESRGAN	21.49	0.6166	20.29	0.6697	20.95	0.6530	22.42	0.5940	22.02	0.5837
RDSR	25.00	0.5196	21.18	0.6167	23.06	0.5586	25.00	0.4993	25.58	0.4814
MM-RealSR	23.49	0.4549	19.74	0.5326	21.76	0.4731	23.37	0.4205	23.97	0.3989
DASR	23.87	0.4683	19.97	0.5752	22.31	0.5093	24.00	0.4474	24.85	0.4225
BSRGAN	23.99	0.4549	20.07	0.5799	22.45	0.4961	24.34	0.4388	24.80	0.4210
RealSRGAN	23.88	**0.4599**	20.10	0.5586	22.12	0.5019	23.85	0.4499	24.48	0.4270
RealSRGAN-TG	**23.95**	0.4617	**21.14**	**0.5323**	**23.06**	**0.4802**	**24.69**	**0.4248**	**25.05**	**0.4112**
RealESRGAN	23.85	0.4325	20.10	0.5355	22.07	0.4701	24.30	0.4147	24.58	0.3970
RealESRGAN-TG	**23.99**	**0.4286**	**21.10**	**0.5056**	**23.15**	**0.4494**	**24.62**	**0.3975**	**25.03**	**0.3851**
RealSwinIR	23.35	0.4468	19.60	0.5624	21.65	0.4905	23.66	0.4265	24.16	0.4077
RealSwinIR-TG	**23.90**	**0.4168**	**20.62**	**0.4925**	**22.70**	**0.4377**	**24.56**	**0.3815**	**24.98**	**0.3670**
RealHAT	24.26	0.4084	20.64	0.5022	22.44	0.4468	24.42	0.3918	25.02	0.3734
RealHAT-TG	**24.31**	**0.4110**	**21.41**	**0.4932**	**23.20**	**0.4395**	**24.87**	**0.3841**	**25.32**	**0.3674**

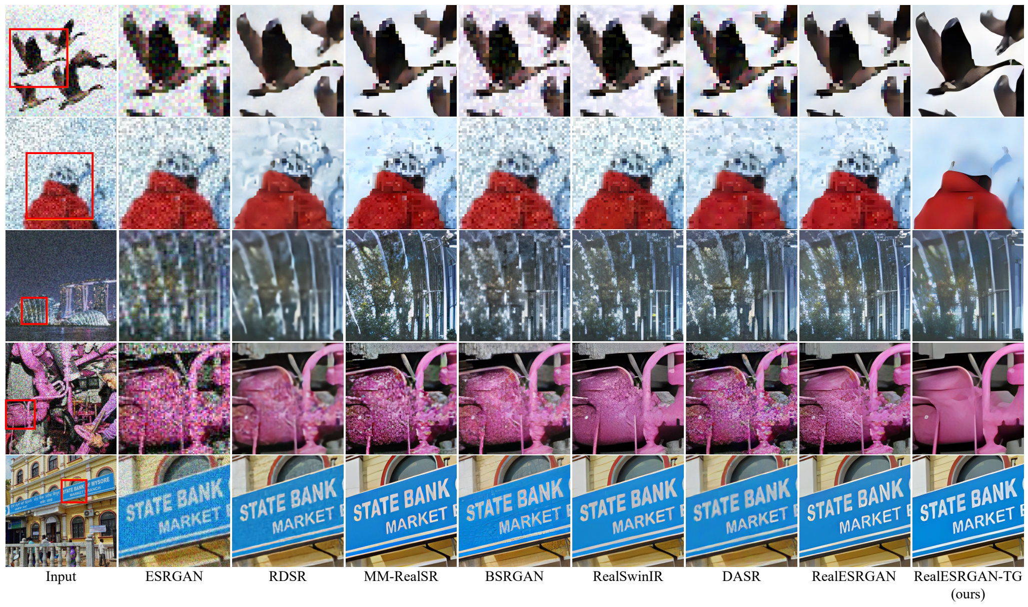

Figure 4: Qualitative results of different methods. Zoom in for details.

RealESRGAN utilize a more complex high-order degradation. As a result, they achieve better LPIPS for real-SR evaluation. However, the two approaches obtain low PSNR performance due to the great difficulty of optimizing. Notably, we can enhance the performance of the pre-trained real-SR network by fine-tuning it on the identified Task Groups (TG). This improvement is particularly significant in Groups 1-4. For instance, on RealESRGAN-TG, we can observe a maximum boost of 1 dB in PSNR and 0.03 in LPIPS.

Our TGSR demonstrates significant superiority when applied to a large degradation space. It is noticeable that RealESRGAN-TG outperforms RealESRGAN even in Group0. This indicates that our approach enhances real-SR performance across nearly the entire degradation space, not just the specifically addressed Groups 1-4. In addition to the identified task groups, our TGSR can also achieve performance gains on the randomized synthetic test sets DIV2K_random and AIM2019 test set as shown in Tab. 2. Additionally, our method achieves a gain on the real scene test set RealSRset. These results clearly demonstrate that our approach does not compromise the performance of certain degradation tasks to enhance the performance of others.

Table 2: Quantitative results of different methods on the real-world test set. The ESRGAN trained on the non-blind setting and RDSR trained on the MSE-based setting are marked in gray.

	DIV2K_random		AIM2019		RealSRset-Nikon		RealSRset-Cano	
	PSNR	LPIPS	PSNR	LPIPS	PSNR	LPIPS	PSNR	LPIPS
ESRGAN	20.63	0.6345	23.16	0.5500	27.40	0.4132	27.73	0.4054
RDSR	24.61	0.5268	24.44	0.4803	26.39	0.4053	26.93	0.3795
MM-RealSR	23.17	0.4394	23.48	0.3917	23.78	0.3841	24.42	0.3664
DASR	23.52	0.4832	23.76	0.4210	26.68	0.3972	27.68	0.3792
BSRGAN	23.76	0.4622	24.20	0.4000	26.11	0.3900	26.90	0.3648
SwinIR	23.13	0.4432	23.89	0.3870	26.20	0.3616	26.68	0.3469
RealESRGAN	23.54	0.4423	23.89	0.3960	25.62	0.3820	26.06	0.3629
RealSRGAN	23.58	0.4710	23.72	0.4247	24.71	0.4159	25.42	0.3902
RealSRGAN-TG	**23.79**	**0.4705**	**23.97**	**0.4174**	**25.18**	**0.4018**	**25.93**	**0.3759**
RealESRGAN	23.54	0.4423	23.89	0.3960	25.62	0.3820	26.06	**0.3629**
RealESRGAN-TG	**23.84**	**0.4368**	**24.27**	**0.3899**	**26.01**	**0.3819**	**26.33**	0.3637
RealSwinIR	23.67	0.4216	23.98	0.3804	25.70	**0.3700**	26.43	**0.3506**
RealSwinIR-TG	**23.74**	**0.4190**	**24.10**	**0.3766**	**26.36**	0.3751	**27.18**	0.3585
RealHAT	24.04	**0.4156**	24.19	0.3742	25.88	**0.3532**	26.56	**0.3339**
RealHAT-TG	**24.21**	0.4189	**24.41**	**0.3723**	**26.12**	0.3635	**26.69**	0.3451

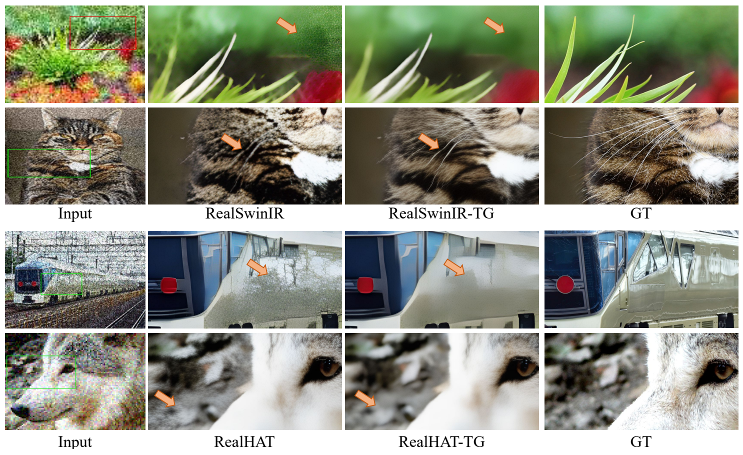

Figure 5: RealSwinIR and RealHAT may unreasonably generate unpleasant artifacts or semantic textures that shouldn't be there. However, our method does not have this problem.

Our TGSR obtains better visual results than other methods. The visual results of different methods are shown in Fig. 4 and Fig. 5. TGSR significantly improves existing methods by removing various degradation artifacts and noticeable unpleasant artifacts. For the first four rows of images with complex degradation, the other methods cannot remove the degradation or generate unacceptable artifacts. In contrast, our TGSR handles the degradation well and produces visually pleasant results. For the image on the last row, our method can generate more realistic results than other methods with clear textures. In the RealSwinIR results of Fig. 5, we can observe the unpleasant artifacts in the flat area of *Flower* image and the fur of *cat* image. In the RealHAT results, we also find semantic textures appearing where they shouldn't be. For example, a *tree* texture appears on the *train*, and fur-like textures are present in the background of the *Wolf* image. However, our method can remove these artifacts by fine-tuning the real-SR network on identified task groups.

5.3 Ablation and Analysis

Effectiveness of the performance indicator. 1) In Fig. 6 (a) and (b), we present the PSNR improvement achieved by fine-tuning the real-SR network on individual tasks with lower and higher performance indicators. It can be observed that tasks with higher performance indicators exhibit a significant PSNR improvement (about 0.4-1.4dB), while tasks with lower performance indicators

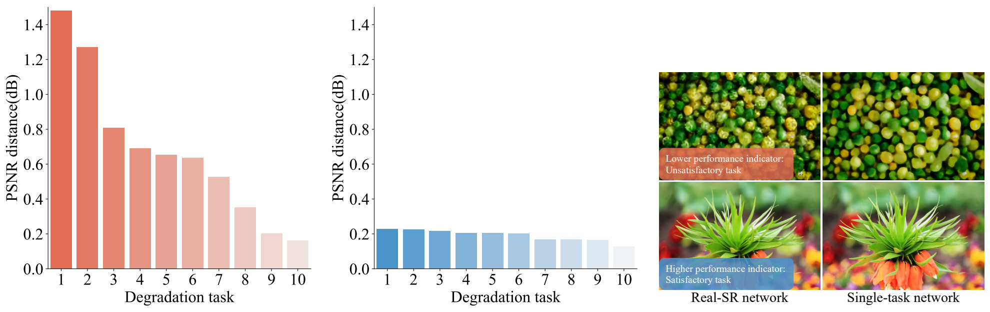

(a) Lower performance indicator (b) Higher performance indicator (c) Visual comparison

Figure 6: Performance comparison of real-SR networks that trained on the degradation tasks with (a) lower performance indicators and (b) higher performance indicators. The degradation tasks with a lower performance indicator can be further improved in quantitative and qualitative results.

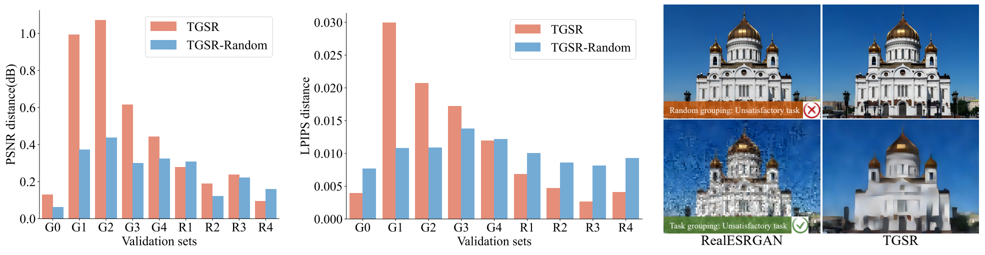

(a) Comparison on PSNR. (b) Comparison on LPIPS. (c) Visual comparison

Figure 7: Performance comparison of RealESRGAN and our TGSR/ TGSR with random grouping on (a) PSNR and (b) LPIPS. The results indicate random grouping achieves limited improvement compared with our proposed task grouping. (c) Visual results demonstrate that random grouping chooses a satisfactory degradation task that is not required for further training, while our task grouping method finds an unsatisfactory degradation task that needs to be further improved.

show only a small PSNR improvement (about 0.2 dB). This finding indicates that our proposed performance indicator can effectively distinguish between satisfactory and unsatisfactory tasks for a real-SR model in a large degradation space. Additionally, Fig. 6 (c) illustrates that significant visual improvements can be achieved with the unsatisfactory degradation task. **2)** Directly fine-tuning a model for each task incurs a high computational cost (empirically requiring at least 10,000 iterations). However, our performance indicator requires only 100 iterations of fine-tuning. It suggests that utilizing the performance indicator can be 100 times faster than direct fine-tuning for distinguishing the unsatisfactory and satisfactory degradation tasks. This further illustrates the superiority of the proposed performance indicator.

Effectiveness of our task grouping algorithm. We compare the performance of RealESRGAN-TG with our task grouping and random grouping to demonstrate the effectiveness of our method. As shown in Fig. 7 (a) and (b), random grouping can only bring very limited performance gains of about 0.2dB on PSNR and about 0.01 on LPIPS. In contrast, the groups generated by our task grouping algorithm show a significant improvement up to 1dB on PSNR and 0.03 on LPIPS. These results demonstrate the significance of a well-designed task grouping approach. Furthermore, Fig. 7 (c) shows that random grouping can not select the unsatisfactory task, while our task grouping algorithm can find it.

Study of the performance upper bound. **(1)** We randomly select 100 single tasks and then add the corresponding small range of similar degradation parameters to each task, named single-task network with range (see details in appendix). Fig. 8 shows that the existence of related tasks can improve the upper bound of some tasks (about 40%). However, there has been a performance drop for other tasks due to similar degradation parameters that may not strictly represent similar tasks. **(2)** To further show the superiority of our TGSR, we fine-tune the RealESRGAN model on each group to obtain

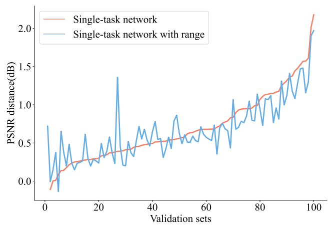

Figure 8: Performance comparison of SR network with a single task and a *range* of tasks.

Table 3: Ablation experiments on the performance upper bound. We fine-tune RealESRGAN directly on each task group to get the corresponding performance upper bound, denoted as RealESRGAN-SG.

Metrics	Model	Group0	Group1	Group2	Group3	Group4
PSNR (↑)	RealESRGAN	23.85	24.58	24.00	22.07	20.10
	RealESRGAN-SG	23.63	24.58	24.39	22.67	20.46
	RealESRGAN-TG (ours)	23.88	25.08	24.62	23.11	21.06
LPIPS (↓)	RealESRGAN	0.4325	0.3970	0.4147	0.4701	0.5355
	RealESRGAN-SG	0.4242	0.3792	0.3929	0.4478	0.4990
	RealESRGAN-TG (ours)	0.4291	0.3845	0.3981	0.4524	0.5087

their empirical performance upper bound for these degradation groups, and the results are denoted as RealESRGAN-SG. As presented in Tab. 3, the fine-tuned models exceed the baseline models and obtain significant performance improvement on LPIPS. Although RealESRGAN-TG cannot surpass the empirical upper bound performance on LPIPS, it still achieves comparable performance. Moreover, our RealESRGAN-TG obtains higher PSNR compared to RealESRGAN-SG. This further shows the superiority of our method and suggests that multi-task learning enhances the performance of the specific task.

Table 4: Quantitative results of different methods on DIV2K8G. Group0 denotes the validation set with satisfactory degradation tasks, and Group1-7 represents the validation sets with unsatisfactory degradation tasks. The ESRGAN trained on the non-blind setting and RDSR trained on the MSE-based setting are marked in gray.

	Metrics	ESRGAN	RDSR	BSRGAN	Real-SwinIR	DASR	MM-RealSR	RealESRGAN	RealESRGAN -TG (ours)
Group0	PSNR (↑)	21.39	25.12	24.19	23.61	23.97	23.61	24.08	**24.10**
	LPIPS (↓)	0.6251	0.5181	0.4567	0.4430	0.4697	0.4335	0.4297	**0.4262**
Group1	PSNR (↑)	19.81	20.99	19.96	19.52	19.77	19.52	19.92	**20.97**
	LPIPS (↓)	0.6812	0.6325	0.6151	0.5954	0.6012	0.5572	0.5584	**0.5249**
Group2	PSNR (↑)	21.10	22.55	21.91	21.16	21.77	21.39	21.67	**22.72**
	LPIPS (↓)	0.6636	0.5755	0.5091	0.4988	0.5175	0.4814	0.4823	**0.4652**
Group3	PSNR (↑)	21.02	23.82	23.24	22.66	23.06	22.54	22.94	**23.93**
	LPIPS (↓)	0.6301	0.5225	0.4657	0.4528	0.4795	0.4445	0.4390	**0.4188**
Group4	PSNR (↑)	22.10	24.64	23.96	23.37	24.05	23.20	23.63	**24.41**
	LPIPS (↓)	0.6221	0.5171	0.4617	0.4429	0.4596	0.4335	0.4294	**0.4097**
Group5	PSNR (↑)	22.78	25.30	24.64	23.99	24.49	23.61	24.36	**25.14**
	LPIPS (↓)	0.5705	0.4873	0.4248	0.4113	0.4245	0.4072	0.4043	**0.3821**
Group6	PSNR (↑)	22.42	25.32	24.58	23.87	24.52	23.71	24.38	**24.86**
	LPIPS (↓)	0.5849	0.4917	0.4255	0.4153	0.4269	0.4060	0.4039	**0.3889**
Group7	PSNR (↑)	22.49	25.37	24.50	23.85	24.43	23.74	24.37	**24.76**
	LPIPS (↓)	0.5868	0.4958	0.4337	0.4227	0.4398	0.4110	0.4083	**0.3976**

Impact of the number of task groups. In Tab. 4, we group the unsatisfactory tasks into more compact new groups using new thresholds of [0.8, 0.7, 0.6, 0.5, 0.4, 0.3, 0.2], with the corresponding number of degradation tasks being [14, 15, 14, 31, 53, 116, 258]. The results demonstrate that our TGSR method exhibits steady improvement on the unsatisfactory tasks in Groups 1-7, while achieving comparable performance on the satisfactory tasks in Group 0. This indicates that our approach can be applied with a more fine-grained division of unsatisfactory tasks based on user requirements.

6 Conclusion

We have re-examined the real-SR problem through the lens of multi-task learning and introduced a novel approach, TGSR, to address task competition in real-SR. TGSR aims to identify and enhance the degradation tasks where a real-SR model underperforms. It involves a task grouping method and a simple fine-tuning approach using the identified task groups. Comprehensive evaluation confirms the effectiveness of our approach in producing high-quality super-resolution results in real-world scenarios. One potential limitation of our method is the need for adequate sampling from the degradation space.

Acknowledgments and Disclosure of Funding

This work was supported in part by the National Natural Science Foundation of China under Grant (62276251,62272450), the Joint Lab of CAS-HK, the National Key RD Program of China (NO. 2022ZD0160100), and in part by the Youth Innovation Promotion Association of Chinese Academy of Sciences (No. 2020356).

References

[1] Eirikur Agustsson and Radu Timofte. Ntire 2017 challenge on single image super-resolution: Dataset and study. In *The IEEE Conference on Computer Vision and Pattern Recognition (CVPR) Workshops*, volume 3, page 2, 2017.

[2] Sefi Bell-Kligler, Assaf Shocher, and Michal Irani. Blind super-resolution kernel estimation using an internal-gan. *Advances in Neural Information Processing Systems*, 32, 2019.

[3] Felix JS Bragman, Ryutaro Tanno, Sebastien Ourselin, Daniel C Alexander, and Jorge Cardoso. Stochastic filter groups for multi-task cnns: Learning specialist and generalist convolution kernels. In *Proceedings of the IEEE/CVF International Conference on Computer Vision*, pages 1385–1394, 2019.

[4] Jianrui Cai, Hui Zeng, Hongwei Yong, Zisheng Cao, and Lei Zhang. Toward real-world single image super-resolution: A new benchmark and a new model. In *Proceedings of the IEEE/CVF International Conference on Computer Vision*, pages 3086–3095, 2019.

[5] Xiangyu Chen, Xintao Wang, Wenlong Zhang, Xiangtao Kong, Yu Qiao, Jiantao Zhou, and Chao Dong. Hat: Hybrid attention transformer for image restoration. *arXiv preprint arXiv:2309.05239*, 2023.

[6] Xiangyu Chen, Xintao Wang, Jiantao Zhou, Yu Qiao, and Chao Dong. Activating more pixels in image super-resolution transformer. In *Proceedings of the IEEE/CVF Conference on Computer Vision and Pattern Recognition*, pages 22367–22377, 2023.

[7] Zhao Chen, Vijay Badrinarayanan, Chen-Yu Lee, and Andrew Rabinovich. Gradnorm: Gradient normalization for adaptive loss balancing in deep multitask networks. In *International conference on machine learning*, pages 794–803. PMLR, 2018.

[8] Zhao Chen, Jiquan Ngiam, Yanping Huang, Thang Luong, Henrik Kretzschmar, Yuning Chai, and Dragomir Anguelov. Just pick a sign: Optimizing deep multitask models with gradient sign dropout. *Advances in Neural Information Processing Systems*, 33:2039–2050, 2020.

[9] Chao Dong, Chen Change Loy, Kaiming He, and Xiaoou Tang. Learning a deep convolutional network for image super-resolution. In *European conference on computer vision*, pages 184–199. Springer, 2014.

[10] Chris Fifty, Ehsan Amid, Zhe Zhao, Tianhe Yu, Rohan Anil, and Chelsea Finn. Efficiently identifying task groupings for multi-task learning. *Advances in Neural Information Processing Systems*, 34:27503–27516, 2021.

[11] Yuan Gao, Haoping Bai, Zequn Jie, Jiayi Ma, Kui Jia, and Wei Liu. Mtl-nas: Task-agnostic neural architecture search towards general-purpose multi-task learning. In *Proceedings of the IEEE/CVF Conference on computer vision and pattern recognition*, pages 11543–11552, 2020.

[12] Yuan Gao, Jiayi Ma, Mingbo Zhao, Wei Liu, and Alan L Yuille. Nddr-cnn: Layerwise feature fusing in multi-task cnns by neural discriminative dimensionality reduction. In *Proceedings of the IEEE/CVF conference on computer vision and pattern recognition*, pages 3205–3214, 2019.

[13] Jinjin Gu, Hannan Lu, Wangmeng Zuo, and Chao Dong. Blind super-resolution with iterative kernel correction. In *Proceedings of the IEEE/CVF Conference on Computer Vision and Pattern Recognition*, pages 1604–1613, 2019.

[14] Yuchao Gu, Xintao Wang, Liangbin Xie, Chao Dong, Gen Li, Ying Shan, and Ming-Ming Cheng. Vqfr: Blind face restoration with vector-quantized dictionary and parallel decoder. In *Computer Vision–ECCV 2022: 17th European Conference, Tel Aviv, Israel, October 23–27, 2022, Proceedings, Part XVIII*, pages 126–143. Springer, 2022.

[15] SHI Guangyuan, Qimai Li, Wenlong Zhang, Jiaxin Chen, and Xiao-Ming Wu. Recon: Reducing conflicting gradients from the root for multi-task learning. In *The Eleventh International Conference on Learning Representations*.

[16] Michelle Guo, Albert Haque, De-An Huang, Serena Yeung, and Li Fei-Fei. Dynamic task prioritization for multitask learning. In *Proceedings of the European conference on computer vision (ECCV)*, pages 270–287, 2018.

[17] Weidong Hu, Wenlong Zhang, Shi Chen, Xin Lv, Dawei An, and Leo Ligthart. A deconvolution technology of microwave radiometer data using convolutional neural networks. *Remote Sensing*, 10(2):275, 2018.

[18] Yan Huang, Shang Li, Liang Wang, Tieniu Tan, et al. Unfolding the alternating optimization for blind super resolution. *Advances in Neural Information Processing Systems*, 33:5632–5643, 2020.

[19] Adrián Javaloy and Isabel Valera. Rotograd: Gradient homogenization in multitask learning. In *ICLR*, 2022.

[20] Alex Kendall, Yarin Gal, and Roberto Cipolla. Multi-task learning using uncertainty to weigh losses for scene geometry and semantics. In *Proceedings of the IEEE conference on computer vision and pattern recognition*, pages 7482–7491, 2018.

[21] Jiwon Kim, Jung Kwon Lee, and Kyoung Mu Lee. Accurate image super-resolution using very deep convolutional networks. In *Proceedings of the IEEE conference on computer vision and pattern recognition*, pages 1646–1654, 2016.

[22] Iasonas Kokkinos. Ubernet: Training a universal convolutional neural network for low-, mid-, and high-level vision using diverse datasets and limited memory. In *Proceedings of the IEEE conference on computer vision and pattern recognition*, pages 6129–6138, 2017.

[23] Xiangtao Kong, Xina Liu, Jinjin Gu, Yu Qiao, and Chao Dong. Reflash dropout in image super-resolution. In *Proceedings of the IEEE/CVF Conference on Computer Vision and Pattern Recognition*, pages 6002–6012, 2022.

[24] Christian Ledig, Lucas Theis, Ferenc Huszár, Jose Caballero, Andrew Cunningham, Alejandro Acosta, Andrew P Aitken, Alykhan Tejani, Johannes Totz, Zehan Wang, et al. Photo-realistic single image super-resolution using a generative adversarial network. In *CVPR*, volume 2, page 4, 2017.

[25] Jie Liang, Hui Zeng, and Lei Zhang. Efficient and degradation-adaptive network for real-world image super-resolution. In *Computer Vision–ECCV 2022: 17th European Conference, Tel Aviv, Israel, October 23–27, 2022, Proceedings, Part XVIII*, pages 574–591. Springer, 2022.

[26] Jingyun Liang, Jiezhang Cao, Guolei Sun, Kai Zhang, Luc Van Gool, and Radu Timofte. Swinir: Image restoration using swin transformer. In *IEEE International Conference on Computer Vision Workshops*, 2021.

[27] Bo Liu, Xingchao Liu, Xiaojie Jin, Peter Stone, and Qiang Liu. Conflict-averse gradient descent for multi-task learning. *Advances in Neural Information Processing Systems*, 34:18878–18890, 2021.

[28] Mingsheng Long, Zhangjie Cao, Jianmin Wang, and Philip S Yu. Learning multiple tasks with multilinear relationship networks. *Advances in neural information processing systems*, 30, 2017.

[29] Andreas Lugmayr, Martin Danelljan, Radu Timofte, Manuel Fritsche, Shuhang Gu, Kuldeep Purohit, Praveen Kandula, Maitreya Suin, AN Rajagoapalan, Nam Hyung Joon, et al. Aim 2019 challenge on real-world image super-resolution: Methods and results. In *2019 IEEE/CVF International Conference on Computer Vision Workshop (ICCVW)*, pages 3575–3583. IEEE, 2019.

[30] Ishan Misra, Abhinav Shrivastava, Abhinav Gupta, and Martial Hebert. Cross-stitch networks for multi-task learning. In *Proceedings of the IEEE conference on computer vision and pattern recognition*, pages 3994–4003, 2016.

[31] Chong Mou, Yanze Wu, Xintao Wang, Chao Dong, Jian Zhang, and Ying Shan. Metric learning based interactive modulation for real-world super-resolution. In *Computer Vision–ECCV 2022: 17th European Conference, Tel Aviv, Israel, October 23–27, 2022, Proceedings, Part XVII*, pages 723–740. Springer, 2022.

[32] Sebastian Ruder. An overview of multi-task learning in deep neural networks. *arXiv preprint arXiv:1706.05098*, 2017.

[33] Sebastian Ruder, Joachim Bingel, Isabelle Augenstein, and Anders Søgaard. Latent multi-task architecture learning. In *Proceedings of the AAAI Conference on Artificial Intelligence*, volume 33, pages 4822–4829, 2019.

[34] Ozan Sener and Vladlen Koltun. Multi-task learning as multi-objective optimization. *Advances in neural information processing systems*, 31, 2018.

[35] Jiayi Shen, Xiantong Zhen, Marcel Worring, and Ling Shao. Variational multi-task learning with gumbel-softmax priors. *Advances in Neural Information Processing Systems*, 34:21031–21042, 2021.

[36] Karen Simonyan and Andrew Zisserman. Very deep convolutional networks for large-scale image recognition. *ICLR*, 2015.

[37] Trevor Standley, Amir Zamir, Dawn Chen, Leonidas Guibas, Jitendra Malik, and Silvio Savarese. Which tasks should be learned together in multi-task learning? In *International Conference on Machine Learning*, pages 9120–9132. PMLR, 2020.

[38] Longguang Wang, Yingqian Wang, Xiaoyu Dong, Qingyu Xu, Jungang Yang, Wei An, and Yulan Guo. Unsupervised degradation representation learning for blind super-resolution. In *Proceedings of the IEEE/CVF Conference on Computer Vision and Pattern Recognition*, pages 10581–10590, 2021.

[39] Xintao Wang, Liangbin Xie, Chao Dong, and Ying Shan. Real-esrgan: Training real-world blind super-resolution with pure synthetic data. In *Proceedings of the IEEE/CVF International Conference on Computer Vision*, pages 1905–1914, 2021.

[40] Xintao Wang, Ke Yu, Chao Dong, and Chen Change Loy. Recovering realistic texture in image super-resolution by deep spatial feature transform. *arXiv preprint arXiv:1804.02815*, 2018.

[41] Xintao Wang, Ke Yu, Shixiang Wu, Jinjin Gu, Yihao Liu, Chao Dong, Chen Change Loy, Yu Qiao, and Xiaoou Tang. Esrgan: Enhanced super-resolution generative adversarial networks. 2018.

[42] Zhang Wenlong, Liu Yihao, Chao Dong, and Yu Qiao. Ranksrgan: Generative adversarial networks with ranker for image super-resolution. *IEEE Transactions on Pattern Analysis and Machine Intelligence*, 2021.

[43] Yanze Wu, Xintao Wang, Gen Li, and Ying Shan. Animesr: Learning real-world super-resolution models for animation videos. In *Advances in Neural Information Processing Systems*.

[44] Liangbin Xie, Xintao Wang, Chao Dong, Zhongang Qi, and Ying Shan. Finding discriminative filters for specific degradations in blind super-resolution. *Advances in Neural Information Processing Systems*, 34:51–61, 2021.

[45] Liangbin Xie, Xintao Wang, Shuwei Shi, Jinjin Gu, Chao Dong, and Ying Shan. Mitigating artifacts in real-world video super-resolution models. *arXiv preprint arXiv:2212.07339*, 2022.

[46] Fanghua Yu, Xintao Wang, Mingdeng Cao, Gen Li, Ying Shan, and Chao Dong. Osrt: Omnidirectional image super-resolution with distortion-aware transformer. *arXiv preprint arXiv:2302.03453*, 2023.

[47] Tianhe Yu, Saurabh Kumar, Abhishek Gupta, Sergey Levine, Karol Hausman, and Chelsea Finn. Gradient surgery for multi-task learning. *Advances in Neural Information Processing Systems*, 33:5824–5836, 2020.

[48] Amir R Zamir, Alexander Sax, William Shen, Leonidas J Guibas, Jitendra Malik, and Silvio Savarese. Taskonomy: Disentangling task transfer learning. In *Proceedings of the IEEE conference on computer vision and pattern recognition*, pages 3712–3722, 2018.

[49] Roman Zeyde, Michael Elad, and Matan Protter. On single image scale-up using sparse-representations. In *International conference on curves and surfaces*, pages 711–730. Springer, 2010.

[50] Kai Zhang, Jingyun Liang, Luc Van Gool, and Radu Timofte. Designing a practical degradation model for deep blind image super-resolution. *arXiv preprint arXiv:2103.14006*, 2021.

[51] Kai Zhang, Wangmeng Zuo, and Lei Zhang. Learning a single convolutional super-resolution network for multiple degradations. In *Proceedings of the IEEE Conference on Computer Vision and Pattern Recognition*, pages 3262–3271, 2018.

[52] Wenlong Zhang, Xiaohui Li, Xiangyu Chen, Yu Qiao, Xiao-Ming Wu, and Chao Dong. Seal: A framework for systematic evaluation of real-world super-resolution. *arXiv preprint arXiv:2309.03020*, 2023.

[53] Wenlong Zhang, Yihao Liu, Chao Dong, and Yu Qiao. Ranksrgan: Generative adversarial networks with ranker for image super-resolution. In *Proceedings of the IEEE/CVF International Conference on Computer Vision*, pages 3096–3105, 2019.

[54] Wenlong Zhang, Guangyuan Shi, Yihao Liu, Chao Dong, and Xiao-Ming Wu. A closer look at blind super-resolution: Degradation models, baselines, and performance upper bounds. In *Proceedings of the IEEE/CVF Conference on Computer Vision and Pattern Recognition*, pages 527–536, 2022.

[55] Yulun Zhang, Kunpeng Li, Kai Li, Lichen Wang, Bineng Zhong, and Yun Fu. Image super-resolution using very deep residual channel attention networks. In *ECCV*, 2018.

[56] Yulun Zhang, Yapeng Tian, Yu Kong, Bineng Zhong, and Yun Fu. Residual dense network for image super-resolution. In *The IEEE Conference on Computer Vision and Pattern Recognition (CVPR)*, 2018.

7 Appendix

7.1 More Details of TGSR

In this section, we provide more training details of our TGSR. As mentioned in the main paper, we follow the RealESRGAN setting to train the real-SR network by standard GAN-based SR loss, including GAN loss L_{GAN}, L1 loss L_1, and perceptual loss L_{per}. The total loss can be defined as follows:

$$\mathcal{L} = w_1 \times \mathcal{L}_{L_1} + w_2 \times \mathcal{L}_{\text{per}} + w_3 \times \mathcal{L}_{\text{GAN}}, \tag{6}$$

The loss weights w_1, w_2, and w_3 are set to 1, 1, and 0.1, respectively. Specifically, for $\mathcal{L}_{L_1}$, we calculate the pixel loss as the L_1 distance $|\hat{y} - y|$, where $\hat{y}$ and y denote the reconstructed HR image and the ground-truth HR image respectively. For the perceptual loss $\mathcal{L}_{\text{per}}$, we extract the conv1, conv2, conv3, conv4, conv5 feature maps of $\hat{y}$ and y using the pre-trained VGG19 network [36], and the loss is calculated as the weighted sum of the respective L_1 distances between the feature maps of $\hat{y}$ and y, with weights set to [0.1, 0.1, 1, 1, 1] for each layer. For the adversarial loss $\mathcal{L}_{\text{GAN}}$, we use a U-Net discriminator with spectral normalization.

7.2 More Ablation Studies and Additional Experimental Results

7.2.1 Impact of the Increased Task Volume

In the main paper, we conducted experiments with a total of 4,000 (4k) degradation tasks. In this subsection, we have increased the number of tasks to 10,000 (10k) by sampling from the degradation space, in order to investigate the impact of the increased task volume on the results. In Fig. 9, we draw the histograms of the performance indicators computed with 4k (a) and 10k (b) degradation tasks respectively. It can be seen that their distributions are quite similar.

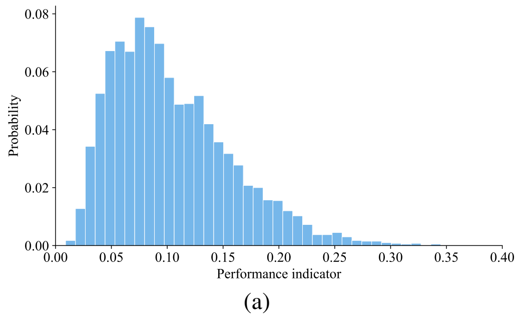

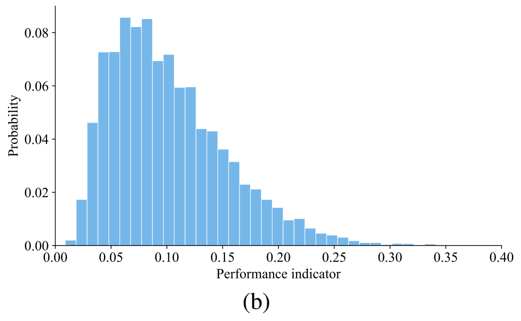

Figure 9: The histograms of the performance indicators with 4k (a) and 10k (b) degradation tasks respectively.

Furthermore, we use the same setup as in the main paper to do task grouping with the 10k degradation tasks and generate the test set for each group. We then compare the performance of TGSR trained with the 10k degradation tasks (TGSR_10k) and the 4k degradation tasks (TGSR_4k). In Tab. 5, we observe that the performance of TGSR_4k on the dataset DIV2K5G_10K is comparable to that of TGSR_10k. This finding suggests that increasing the number of tasks from 4,000 to 10,000 does not lead to significant improvements in performance for TGSR.

7.2.2 Necessity of Iterative Task Grouping

In Tab. 6, we provide the changes in performance improvement scores for various tasks across four training loops in the task grouping process in Alg. 1. It can be observed that many tasks show variations in their performance improvement scores across different training loops. For example, degradation task 5 exhibits a performance improvement of 0.57dB in the first training loop and 0.72dB in the third loop. This suggests that certain tasks are given priority during training in each loop, which leads to limited performance improvement for other tasks due to task competition. The observation supports the necessity of iterative task grouping as outlined in Alg. 1.

Table 5: Quantitative results of TGSR trained with the 4k and 10k degradation tasks, respectively. Group0 denotes the validation set with satisfactory degradation tasks, and Group1-4 represents the validation sets with unsatisfactory degradation tasks. The suffix 4k and 10k represent groups generated with the 4k and 10k degradation tasks, respectively.

	Metrics	Group0_4k	Group1_4k	Group2_4k	Group3_4k	Group4_4k
RealESRGAN	PSNR (↑)	23.85	20.11	22.08	24.00	24.59
	LPIPS (↓)	0.4325	0.5355	0.4701	0.4147	0.3970
RealESRGAN-TG_4k	PSNR (↑)	23.98	21.10	23.15	24.62	25.03
	LPIPS (↓)	0.4286	0.5056	0.4494	0.3975	0.3851
RealESRGAN-TG_10k	PSNR (↑)	23.91	21.03	22.98	24.50	24.97
	LPIPS (↓)	0.4299	0.5064	0.4525	0.4002	0.3859
	Metrics	Group0_10k	Group1_10k	Group2_10k	Group3_10k	Group4_10k
RealESRGAN	PSNR (↑)	23.81	19.85	20.95	23.77	24.38
	LPIPS (↓)	0.4324	0.5495	0.5073	0.4237	0.4019
RealESRGAN-TG_4k	PSNR (↑)	24.12	20.90	21.85	24.38	25.03
	LPIPS (↓)	0.4272	0.5187	0.4890	0.4046	0.3875
RealESRGAN-TG_10k	PSNR (↑)	24.05	20.94	21.85	24.31	24.93
	LPIPS (↓)	0.4285	0.5171	0.4907	0.4052	0.3886

Table 6: Performance improvement score of some degradation tasks across four training loops. NA means that the task is not available, since it has been grouped in the previous loop.

Training loop	Deg.1	Deg.2	Deg.3	Deg.4	Deg.5	Deg.6	Deg.7	Deg.8	Deg.9	Deg.10
Train1	0.45	1.50	0.60	0.66	0.57	0.75	0.55	0.60	0.61	0.46
Train2	0.47	NA	0.63	0.67	0.41	0.76	0.49	0.59	0.64	0.48
Train3	0.48	NA	NA	NA	0.72	NA	0.65	0.63	NA	0.48
Train4	NA	NA	NA	NA	NA	NA	NA	NA	NA	NA
Degradation	Deg.11	Deg.12	Deg.13	Deg.14	Deg.15	Deg.16	Deg.17	Deg.18	Deg.19	Deg.20
Train1	0.43	0.60	0.47	0.27	0.66	0.53	0.22	0.31	0.63	0.20
Train2	0.42	0.59	0.47	0.33	0.51	0.52	0.18	0.31	0.67	0.21
Train3	0.48	0.63	0.50	0.31	0.73	0.54	0.18	0.37	NA	0.25
Train4	NA	NA	NA	0.35	NA	NA	0.23	0.46	NA	0.26

7.2.3 Comparison with Single-task Network

It is commonly believed that a single-task network fine-tuned specifically for a particular degradation task can achieve the upper bound of performance for that task. However, in Fig. 10, we compare the PSNR improvement over RealESRGAN between our TGSR and the single-task network on a set of randomly selected tasks. Interestingly, we observe that the performance of the single-task network even decreases for tasks 1 and 4 in terms of PSNR, while our TGSR, which utilizes task grouping for multi-task learning, consistently improves performance across all tasks. On average, TGSR achieves a PSNR improvement of 0.74dB and an LPIPS improvement of 0.04, whereas the single-task network only achieves a PSNR improvement of 0.30dB and an LPIPS improvement of 0.03. This demonstrates the effectiveness of the task grouping and multi-task learning strategy in TGSR, which leverages the shared information across tasks to improve the generalization ability of the model and achieve better overall performance.

7.2.4 Impact of the Increased Volume of Unsatisfactory Tasks

Tab. 7 presents the results of TGSR with additional unsatisfactory tasks. We categorize the unsatisfied tasks into 9 groups based on thresholds [0.8, 0.7, 0.6, 0.5, 0.4, 0.3, 0.2, 0.15, 0.1] (0.15 and 0.1 are used to include more unsatisfactory tasks compared to Tab. 4), with the corresponding number of degradation tasks as [14, 15, 14, 31, 53, 116, 258, 190, 206]. We can observe that TGSR consistently achieves performance improvement on the unsatisfactory tasks in Groups 1-9 while maintaining comparable results on the satisfactory tasks in Group 0. It is worth noting that as the threshold for dividing the groups decreases, the performance gain becomes gradually smaller.

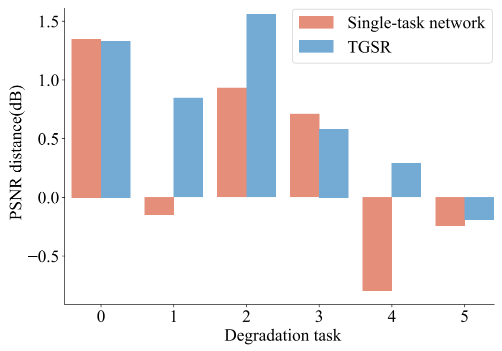

(a) Performance comparison in PSNR.

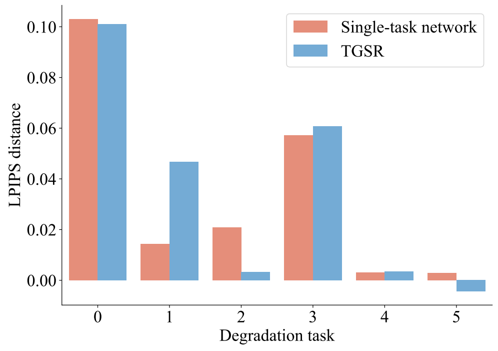

(b) Performance comparison in LPIPS.

Figure 10: Performance comparison of single-task network and TGSR in (a) PSNR and (b) LPIPS.

Table 7: Quantitative results of different methods on DIV2K10G. Group0 denotes the validation set with satisfactory degradation tasks, and Group1-9 represents the validation sets with unsatisfactory degradation tasks.

	Metrics	ESRGAN	RDSR	BSRGAN	RealSwinIR	DASR	MM-RealSR	RealESRGAN	RealESRGAN-TG (ours)
Group0	PSNR (↑)	21.15	24.80	23.66	22.97	23.66	23.28	23.65	**23.78**
	LPIPS (↓)	0.6268	0.5255	0.4616	0.4503	0.4743	0.4403	0.4358	**0.4344**
Group1	PSNR (↑)	20.01	21.13	20.07	19.62	19.85	19.63	20.01	**21.07**
	LPIPS (↓)	0.6708	0.6267	0.6051	0.5834	0.5923	0.5552	0.5563	**0.5188**
Group2	PSNR (↑)	21.08	22.38	21.82	20.97	21.53	21.06	21.36	**22.47**
	LPIPS (↓)	0.6687	0.5821	0.5177	0.5092	0.5200	0.4910	0.4922	**0.4735**
Group3	PSNR (↑)	20.94	23.58	23.06	22.40	22.82	22.30	22.72	**23.58**
	LPIPS (↓)	0.6421	0.5410	0.4809	0.4671	0.4940	0.4564	0.4553	**0.4393**
Group4	PSNR (↑)	22.10	24.80	24.27	23.56	24.31	23.46	23.82	**24.40**
	LPIPS (↓)	0.6098	0.5082	0.4470	0.4326	0.4496	0.4257	0.4238	**0.4047**
Group5	PSNR (↑)	22.84	25.58	24.89	24.27	24.91	23.85	24.56	**25.07**
	LPIPS (↓)	0.5626	0.4843	0.4208	0.4057	0.4187	0.4009	0.3974	**0.3768**
Group6	PSNR (↑)	22.50	25.11	24.39	23.72	24.42	23.64	24.10	**24.63**
	LPIPS (↓)	0.5895	0.4979	0.4400	0.4254	0.4410	0.4161	0.4130	**0.3993**
Group7	PSNR (↑)	22.41	25.54	24.72	24.03	24.44	23.80	24.50	**24.90**
	LPIPS (↓)	0.5884	0.4892	0.4248	0.4146	0.4341	0.4048	0.4016	**0.3897**
Group8	PSNR (↑)	20.94	25.08	24.19	23.57	23.77	23.44	24.10	**24.52**
	LPIPS (↓)	0.6223	0.5057	0.4492	0.4354	0.4568	0.4226	0.4211	**0.4112**
Group9	PSNR (↑)	19.86	24.89	23.85	23.29	23.65	23.44	23.97	**24.29**
	LPIPS (↓)	0.6340	0.5140	0.4624	0.4485	0.4820	0.4333	0.4302	**0.4209**

7.3 More Visual Results

Fig. 11 presents additional sample images from our validation datasets, including some unsatisfactory degradation tasks from Groups 1-4 and some satisfactory degradation tasks from Group 0. These images are accompanied by the corresponding ground-truth images. Fig. 12 presents an additional qualitative comparison of competing methods on DIV2K5G. Fig. 13 presents an additional qualitative comparison of competing methods on real-world images. Through the grouping and handling of unsatisfactory degradation tasks, our TGSR exhibits enhanced generalization ability when applied to real-world images.

7.3.1 More Sample Images in DIV2K5G

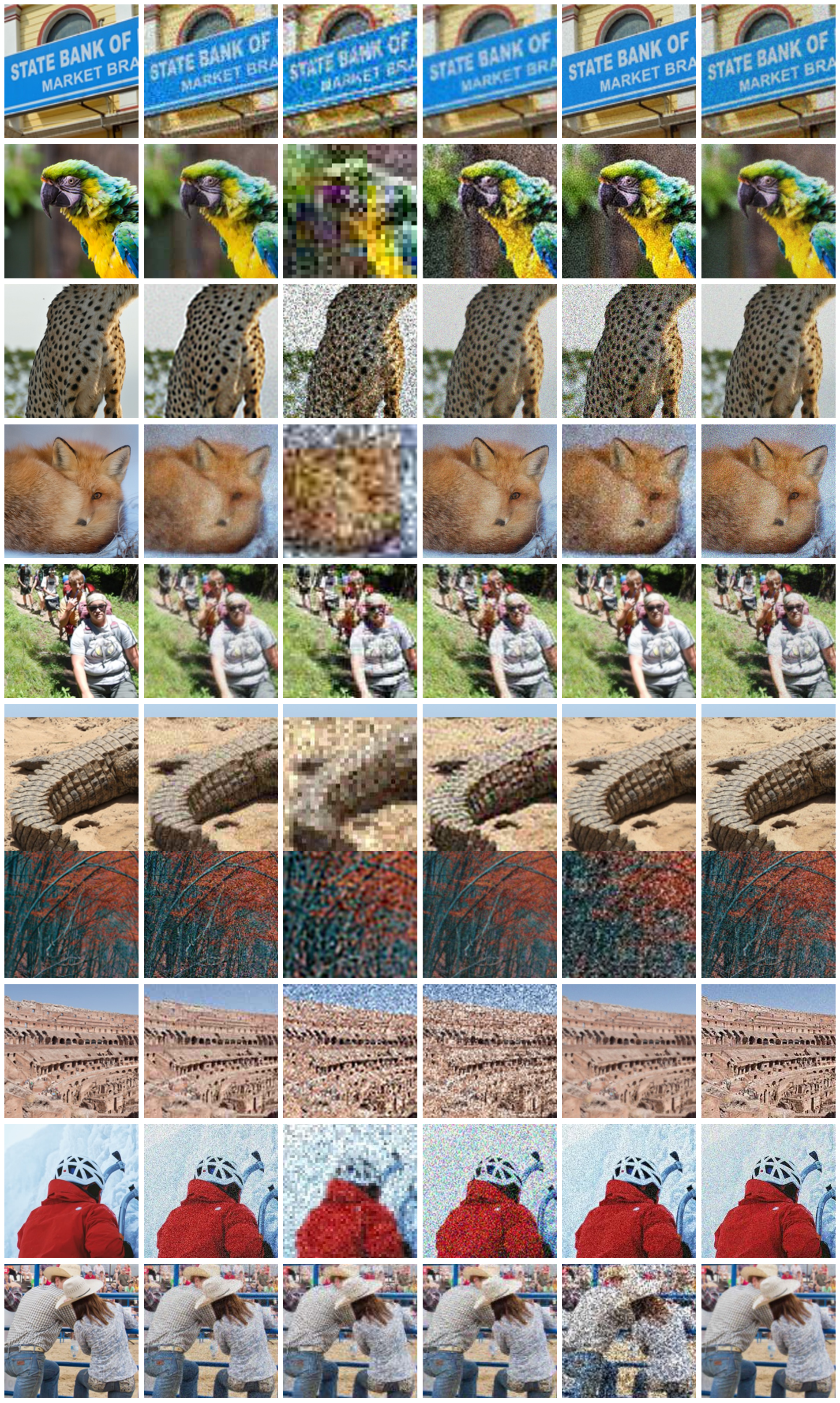

Figure 11: Sample images from different degradation task groups in our DIV2K5G datasets.

7.3.2 More Qualitative Comparisons on DIV2K5G

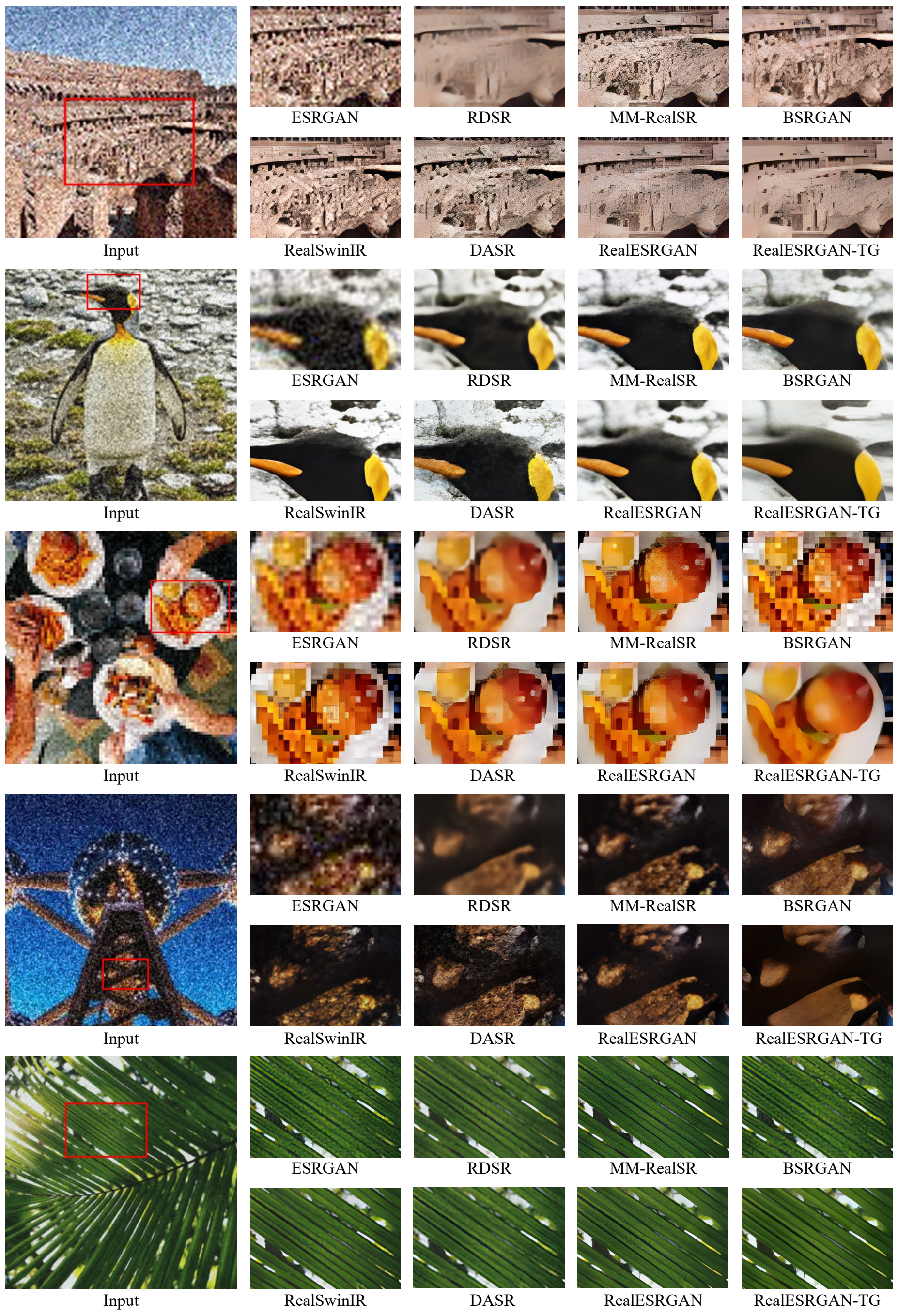

Figure 12: Qualitative comparison of competing methods on DIV2K5G.

7.3.3 More Qualitative Comparisons on Real-world Images

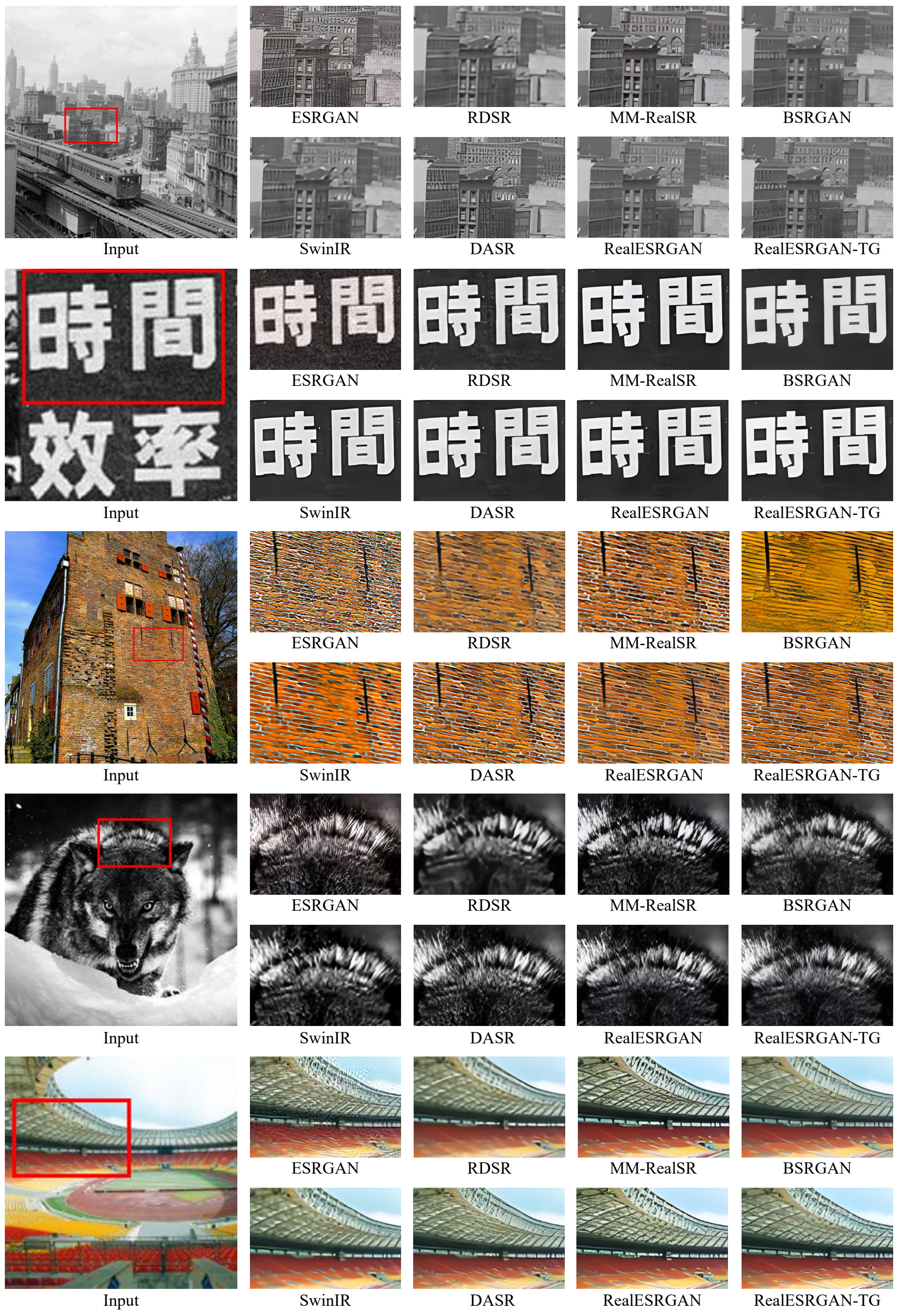

Figure 13: Qualitative comparison of competing methods on real-world images.